Two-wave mixing in (111)-cut $Bi_{12}SiO_{20}$ and $Bi_{12}TiO_{20}$ crystals: Characterization and comparison with the general orientation

V. P. Kamenov, Yi Hu, E. Shamonina, and K. H. Ringhofer
Department of Physics, University of Osnabrück, D-49069 Osnabrück, Germany

V. Ya. Gayvoronsky
Institute of Physics, National Academy of Sciences, 252650 Kiev, Ukraine
(Received 20 December 1999)

We study the process of two-wave mixing (TWM) in optically active, electro-optic, and elasto-optic BSO and BTO crystals. We calculate the TWM gain for arbitrary crystal cut and optimize the energy exchange. For the (111) cut, by choosing an appropriate coordinate system, we obtain a simple analytical solution for the components of the coupling tensor which allows us to optimize analytically the TWM gain with respect to the grating orientation and the initial light polarization.

PACS number(s): 42.70.Nq, 42.65.Hw

I. INTRODUCTION

The energy exchange of TWM in sillenite crystals is the subject of many studies. In these crystals, in addition to the primary electro-optic (Pockels) effect, there exists also the elasto-optic effect (or secondary electro-optic effect) as well as optical activity. It is known that optical activity affects TWM strongly [1,2]. After the pioneering work of Izvanov *et al.* [3], the role of the elasto-optic effect for sillenite crystals was investigated intensively [4–22]. Recently, it was shown that the elasto-optic effect leads to surface relief gratings [19] and to surface waves [20]. In most of the TWM studies in sillenites the intermediate role of all three effects mentioned above must be considered.

For real-time holographic interferometry in sillenites under diffusion recording [23], it is important to optimize the energy exchange. Many papers were devoted to such an optimization [5,6,8–10,13,17,18,21,22]. They show that the influence of optical activity and of the elasto-optic effect is significant. Nevertheless, for a long time there was a widespread belief that the optimum orientation is obtained for the grating orientation $\mathbf{K} \| [111]$ (and for polarization [111] of the recording beams) since both the electro-optic and elasto-optic effect are most pronounced along the space diagonal of the unit cell [4]. In Refs. [18] and [21] the simultaneous influence of optical activity and of the elasto-optic and electro-optic effect is investigated for (110)-cut crystals. It is shown that owing to the natural optical activity in sillenites the optimum grating orientation, as well as the optimum light polarization, moves away from the [111] direction and depends strongly on the crystal thickness. Corresponding results were obtained later for the (111) cut [22]. These recent results question the most popular cut (110) as the optimum one so that a detailed study of two-wave mixing with arbitrary crystal orientation involving all known effects is necessary. Reference [17] makes an attempt to treat this problem analytically. However, the considerations there are very general and do not give a clear answer.

In order to give an overall picture we derive the general orientational dependence of the gain for crystals with point group symmetry (23) (in particular BSO and BTO) and optimize it, taking into account optical activity as well as the elasto-optic and electro-optic effect.

In the last few years there was a growing interest in (111)-cut crystals as photorefractive medium in TWM and four-wave mixing experiments [22,24–27]. The authors of Ref. [24] show that the diffraction efficiency for *s*-polarized waves in (111)-cut GaAs crystals does not depend on the grating orientation. In this work the elasto-optic effect is neglected. The dependence of the TWM gain for *s*- and *p*-polarized waves on the grating orientation in the (111) plane without taking into account optical activity and the elasto-optic effect is given in Ref. [27]. It is shown in Ref. [25] that reflexion gratings in (111)-cut BSO crystals can be used for dynamic interferometry, whereby it is possible to write a grating by orthogonally polarized waves. The optimization of the TWM gain for (111)-cut BSO crystals is given in Ref. [22]. However, the expressions given there are quite complicated and it is difficult to understand their physical meaning. It is a common disturbing feature of the elasto-optic effect that the dependence of its contribution to the photorefractivity on the grating orientation can become very complicated.

In this paper we give a simple analytical expression for the coupling tensor of a (111)-cut crystal which simplifies the propagation equations significantly. This allows us to describe TWM under diffusion recording in optically active, electro-optic and elasto-optic BSO and BTO crystals analytically and to present the optimal gain with respect to the grating orientation and the initial light polarization in a simple form.

The structure of the paper is as follows. In Sec. II we present the coupled wave equations for TWM in sillenites under diffusion recording. Sec. III optimizes the gain for general crystal orientation. In Sec. IV we stress the special cut (111) and characterize its coupling tensor and its gain analytically.

II. COUPLED WAVE EQUATIONS

In our considerations a pump wave $\mathbf{E}_p \exp[i(\mathbf{k}_p \cdot \mathbf{r} - \omega t)]$ and a signal wave $\mathbf{E}_s \exp[i(\mathbf{k}_s \cdot \mathbf{r} - \omega t)]$ interact in an arbi-

trarily oriented sillenite crystal. We assume that the incidence angles of both waves are equal and small so that the amplitudes $\mathbf{E}_p$ and $\mathbf{E}_s$ have only x and y components and the grating vector $\mathbf{K}=\mathbf{k}_p-\mathbf{k}_s$ lies in the xy-plane. In this paraxial approximation the waves themselves propagate through the medium along an arbitrary z direction.

The coupled wave equations for the slowly varying amplitudes $\mathbf{E}_p$ and $\mathbf{E}_s$ in the steady state have the form

$$\mathbf{E}_s'=i\varrho\,\boldsymbol{\sigma}_2\cdot\mathbf{E}_s+ig^*\mathbf{H}\cdot\mathbf{E}_p\,,$$

$$\mathbf{E}_p'=i\varrho\,\boldsymbol{\sigma}_2\cdot\mathbf{E}_p+ig\mathbf{H}\cdot\mathbf{E}_s\,,$$

(1)

where ϱ is the rotatory power, $\boldsymbol{\sigma}_2$ is the 2nd component of the vector of Pauli matrices, $\mathbf{H}$ is the coupling tensor (with dimensionless components), and g is the coupling constant, proportional to the space-charge field E_{sc}. For diffusion recording

$$g=i\Gamma\frac{m}{2}=-\frac{\pi n^3 r_{41}^S}{\lambda}E_{sc}\,,\quad \Gamma=\frac{\pi n^3 r_{41}^S}{\lambda}\frac{Kk_BT/e}{1+(Kr_D)^2}\,,$$

(2)

where $m=2\mathbf{E}_s^*\cdot\mathbf{E}_p/(|\mathbf{E}_s|^2+|\mathbf{E}_p|^2)$ is the complex light modulation depth, n the refractive index, r_{41}^S the clamped electro-optic coefficient, λ the wavelength, $r_D=(\bar{\epsilon}\epsilon_0 k_B T/N_t e^2)^{1/2}$ the Debye radius, k_B Boltzmann's constant, T the temperature, e the electron charge, $\bar{\epsilon}\epsilon_0$ the dielectric permittivity, N_t the effective trap density, and $K=|\mathbf{K}|$.

The coupling tensor $\mathbf{H}$ is proportional to the induced change of the inverse dielectric permittivity tensor, $\mathbf{H}=-\Delta\boldsymbol{\epsilon}^{-1}/(r_{41}^S E_{sc})$. The changes of $\boldsymbol{\epsilon}^{-1}$ are via the linear electro-optic effect and the elasto-optic effect,

$$\Delta\epsilon_{ij}^{-1}=E_{sc}(r_{ijq}^S+p_{ijkl}\gamma_{kn}e_{qnm}n_l n_m)n_q\,,$$

(3)

where the tensor γ_{kn} is the inverse of the Christoffel tensor $\Gamma_{kn}=c_{kinj}^E n_i n_j$; by r_{ijq}^S, p_{ijkl}, c_{kinj}^E, and e_{qnm} we denote the components of the linear electro-optic, elasto-optic, elasticity, and piezoelectric tensors, respectively; (n_1,n_2,n_3) are the components of the unit vector $\mathbf{K}/K$ pointing in the direction of the grating vector in the crystallographic coordinate system. The second term in Eq. (3) corresponds to the contribution of the elasto-optic effect: (i) the space-charge field creates stress in the crystal through the inverse piezoelectric effect (e_{qnm}); (ii) consequently, the crystal is deformed by Hooke's law with elastic moduli (c_{kinj}^E); (iii) finally, the deformations change the inverse dielectric permittivity tensor (p_{ijkl}).

Performing the multiplications in Eq. (3) we obtain for the components of $\Delta\boldsymbol{\epsilon}^{-1}$ in the crystallographic coordinate system,

$$\Delta\epsilon_{ij}^{-1}=E_{sc}r_{41}^S n_s+E_{sc}Gp_4\{An_i^2 n_j^2+B(n_i^2+n_j^2)$$
$$+C(n_i^4+n_j^4)n_s^2+Dn_1^2 n_2^2 n_3^2\}n_s\,,$$

(4)

$$\Delta\epsilon_{ii}^{-1}=E_{sc}G\{B(p_1+p_2+p_3)+E(p_1 n_i^2+p_2 n_j^2+p_3 n_s^2)$$
$$+F(p_1 n_i^4+p_2 n_j^4+p_3 n_s^4)+C(p_1 n_j^2 n_s^2+p_2 n_s^2 n_i^2$$
$$+p_3 n_i^2 n_j^2)\}n_1 n_2 n_3\,,$$

with

$$A=-(c_2+c_4)(c_1-c_2+2c_4)-2c_4(c_1-c_4)\,,$$

$$B=c_1 c_4\,,$$

$$C=(c_1+c_2)(c_1-c_2-2c_4)\,,$$

$$D=-(c_2+c_4)(c_1-c_2-2c_4)\,,$$

$$E=-(c_2+c_4)(c_1-c_2)-c_4(c_1-c_4)\,,$$

$$F=(c_2+c_4)(c_1-c_2-2c_4)\,,$$

$$G=2e_{41}\{c_1 c_4^2+(c_1+2c_2+c_4)(c_1-c_2-2c_4)^2 n_1^2 n_2^2 n_3^2$$
$$+c_4(c_1+c_2)(c_1-c_2-2c_4)(n_1^2 n_2^2+n_1^2 n_3^2+n_2^2 n_3^2)\}^{-1}\,.$$

Here the indices $\{ijs\}$ are cyclic permutations of the sequence $\{123\}$; the parameters $(p_1,p_2,p_3,p_4)=(p_{11}^E,p_{12}^E,p_{13}^E,p_{44}^E)$, $(c_1,c_2,c_4)=(c_{11}^E,c_{12}^E,c_{44}^E)$, and e_{41} are the nonzero components of the elasto-optic, elastic, and piezoelectric tensors, respectively. Note that the electro-optic effect contributes only to the off-diagonal elements of $\Delta\boldsymbol{\epsilon}^{-1}$ [see the first term on the right-hand side of $\Delta\epsilon_{ij}^{-1}$ in Eq. (4)].

To calculate the coupling tensor $\mathbf{H}$, we need to transform $\Delta\boldsymbol{\epsilon}^{-1}$ to the laboratory coordinate system with the z-axis coinciding with the propagation direction of the light,

$$H_{ij}=-\frac{1}{r_{41}^S E_{sc}}\mathbf{e}_i\cdot\Delta\boldsymbol{\epsilon}^{-1}\cdot\mathbf{e}_j\,,\quad i=x,y,\quad j=x,y,\quad (5)$$

where $\mathbf{e}_{x,y}$ are the unit vectors along the x and y axes of the laboratory coordinate system. In contrast to the z-direction, which is determined from the crystal cut, the choice of $\mathbf{e}_{x,y}$ is free.

III. OPTIMIZATION FOR ARBITRARY CRYSTAL CUT

In this section we optimize the energy exchange between the pump and the signal beam at a given crystal thickness by varying the direction of light propagation (i.e., the crystal cut), the grating orientation, and the light polarization. We consider sillenite crystals which are optically active and piezoelectric. The optical absorption is neglected because it has no influence on the gain, G,

$$G=\frac{|\mathbf{E}_s|^2-|\mathbf{E}_s^0|^2}{|\mathbf{E}_s^0|^2}\,,$$

(6)

where $\mathbf{E}_s^0$ is the signal beam amplitude in the absence and $\mathbf{E}_s$ the corresponding amplitude in the presence of the pump beam, both values being measured behind the crystal.
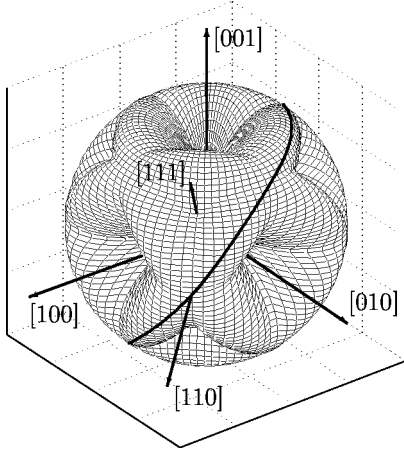
FIG. 1. Orientational dependence of the normalized maximal effective coupling, C_{eff}, for BSO. The maximal effective coupling for a given cut is drawn in the direction of the normal to the crystal surface.

In our calculations the pump and the signal waves are linearly polarized with the same input polarization, which is one of the conditions for the strongest coupling of the waves [17]. Choosing $K = r_D^{-1}$ we ensure that the space-charge field in the crystal has the largest possible amplitude with respect to the angle of incidence [1].

The crystal parameters used in the calculations below are [18]: $\lambda = 514.5$ nm, $n = 2.615$, $\bar{\epsilon} = 56$, $\varrho = 38.6°/mm$, $r_{41}^S = 5.0 \times 10^{-12}$ m/V, $e_{41} = 1.12$ C/m², $c_{\{1,2,4\}} = \{12.96, 2.99, 2.45\} \times 10^{10}$ N/m², $p_{\{1,2,3,4\}} = \{0.16, 0.13, 0.12, 0.015\}$, and $N_t = 10^{22}$ m⁻³ for BSO; $\lambda = 633$ nm, $n = 2.58$, $\bar{\epsilon} = 47$, $\varrho = 6.3°/mm$, $r_{41}^S = 4.75 \times 10^{-12}$ m/V, $e_{41} = 1.1$ C/m², $c_{\{1,2,4\}} = \{13.7, 2.8, 2.6\} \times 10^{10}$ N/m², $p_{\{1,2,3,4\}} = \{0.173, -0.0015, -0.0015, -0.005\}$, and $N_t = 10^{22}$ m⁻³ for BTO.

A. TWM without optical activity

Let us now neglect optical activity, i.e., we consider a very thin crystal. For TWM in an optical nonactive medium, under diffusion recoding the interacting waves keep their initial linear polarization. The additional rotation of the light polarization caused from the nonlinear interaction of the waves can also be neglected because the crystal is thin.

Examining Eqs. (1) for $\varrho = 0$ one can see that the only parameter responsible for the optimization of the energy exchange is the so called effective coupling [27],

$$C_{eff} = \mathbf{e}_s \cdot \mathbf{H} \cdot \mathbf{e}_p, \qquad (7)$$

where $\mathbf{e}_p$ and $\mathbf{e}_s$ are the polarization vectors corresponding to the wave amplitudes $\mathbf{E}_p$ and $\mathbf{E}_s$ (in our treatment $\mathbf{e}_s \equiv \mathbf{e}_p$).

From Eqs. (4), (5), and (7) we calculate the effective coupling for arbitrary crystal orientation. In order to get the strongest energy exchange for every cut we maximize C_{eff} with respect to all grating orientations and all light polarization vectors in the xy plane (remember that in our paraxial approximation the z-axis coincides always with the propagation direction).

In Fig. 1 the maximal coupling coefficient for each crystal cut is drawn in the direction of the surface normal of this cut

for a BSO crystal (for BTO the dependence is qualitatively the same). The symmetry of the figure corresponds to the symmetry of the point group (23). In cubic crystals the space diagonal (e.g., [111]) has threefold symmetry, which can be clearly seen from the figure. The twofold symmetry of the diagonal of one of the cube faces (e.g., [110]) is also well emphasized. The basic symmetry for the crystallographic axes [100], [010], and [001] is twofold. Higher symmetry is not forbidden, and these axes show fourfold symmetry. The absolute minimum (namely zero) occurs when the light propagates along one of the crystallographic axes [100], [010], and [001]. In this case the waves are not coupled at all. The absolute maximum is achieved for the cut with $\mathbf{e}_z \| [110]$. In order to explain this, we recall that for this crystal cut the grating vector $\mathbf{K}$ and the $[1\bar{1}1]$-direction lie in the same plane. Consequently, the grating can be oriented along the space diagonal, which is the condition for maximal energy exchange if there is no optical activity. Actually all propagation directions which lie in the plane perpendicular to one of the four space diagonals of the cube fulfill this condition and give maximal coupling (see the bold curve in Fig. 1). An additional feature of Fig. 1 is that there is a local minimum which appears when $\mathbf{e}_z$ is parallel to [111] (or to any other space diagonal).

B. TWM with optical activity

For diffusion recording, optical activity in sillenite crystals can usually not be neglected. Without applied external field the initial linear polarizations of the light waves remains linear within the crystal but their angles of polarization change strongly with the crystal thickness owing to natural optical activity. Since it is impossible to keep the optimum polarization everywhere inside the crystal, the effective coupling alters periodically with the thickness. The resulting energy exchange will not reach the maximum value possible for an optically nonactive crystal because the maximal effective coupling can be achieved only locally. Correspondingly, as shown for the (110) cut, the optimum grating orientation is generally not in the [111] direction [18]. Here we will additionally optimize the TWM gain with respect to the crystal orientation. For any given propagation direction we look for grating orientation and initial polarization angles for which the energy exchange between the beams becomes maximum.

Including optical activity in Eqs. (1) makes the optimization more mathematically complicated. In our analysis we use the approximation of constant light modulation along the crystal thickness and the approximation of strong optical activity. The argument for the first approximation is that the diffraction efficiency in sillenites is small enough so that the dynamic change of the light modulation is negligible. The validity of the second approximation is based on the value of the ratio $\tilde{g}/\varrho$, with $\tilde{g} = \Gamma \beta/(\beta + 1)$, where β is the beam intensity ratio. For typical BSO parameters we find $\tilde{g}/\varrho = 0.06$ ($\beta = 1$) and $\tilde{g}/\varrho = 0.12$ ($\beta \to \infty$) so that optical activity dominates. For BTO, $\tilde{g}/\varrho$ is in the range from 0.23 ($\beta = 1$) to 0.57 ($\beta \to \infty$) so that we may only expect qualitative agreement with experiment.

The practical consequences of the above approximations are that (i) g is constant along the crystal width; (ii) the
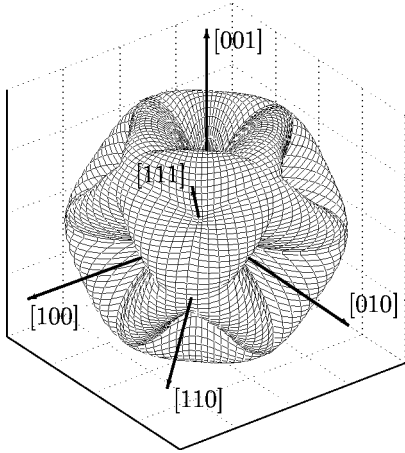
FIG. 2. Orientational dependence of the normalized optimum gain for BSO at $\varrho d = 180°$ (see the caption of Fig. 1).

eigenmodes of the system are (left or right) circularly polarized waves. Using (i) and (ii) we obtain,

$$G = \Gamma d \frac{\beta}{\beta+1} [(H_{11}+H_{22}) + (H_{11}-H_{22})\tau\cos(2\varphi-\varrho d)$$
$$+ 2H_{12}\tau\sin(2\varphi-\varrho d)], \qquad (8)$$

with

$$\tau = \sin(\varrho d)/(\varrho d).$$

Here d is the crystal thickness, and φ is the polarization angle measured from the x axis of the laboratory coordinate system. For the first time an analytical expression of this form for the gain was given in Ref. [18] but it was not realized there that it is even valid for an arbitrary crystal cut if only the coupling tensor components and the polarization angle are measured in the appropriate coordinate system.

The strongest influence of optical activity on the TWM process is to be expected when the polarization vector rotates by 180° during the propagation in the crystal and doing so scans all possible angles of polarization. In this case the resulting gain is independent of the initial light polarization. We have seen that (110) is the optimum cut without optical activity. It can be expected that the strongest shift of the optimum crystal orientation from (110) is at $\varrho d = 180°$ [18,21]. The optimization of Eq. (8) for BSO for $\varrho d = 180°$ is shown in Fig. 2 (for BTO we obtain qualitatively the same dependence). The symmetry of Fig. 1 is here present again. The absolute and local minima (e.g., $\mathbf{e}_z\|[001]$ and $\mathbf{e}_z\|[111]$, respectively) are preserved too. Contrary to the case $\varrho=0$, the propagation directions perpendicular to [111] are no longer equivalent. Before all the planes perpendicular to the space diagonals gave the propagation directions which correspond to the absolute maximum of the gain. Now there are only six equivalent maxima: $[110]$, $[1\bar{1}0]$, $[01\bar{1}]$, $[10\bar{1}]$, $[101]$, and $[011]$. It is interesting to note that the optimization gives the same result for each $\varrho d > 0$. In general, the closer ϱd is to 180° the bigger the difference is between the maximum gain for $[110]$ and the other propagation directions perpendicular to one of the space diagonals of the cell. That is, (110) remains the
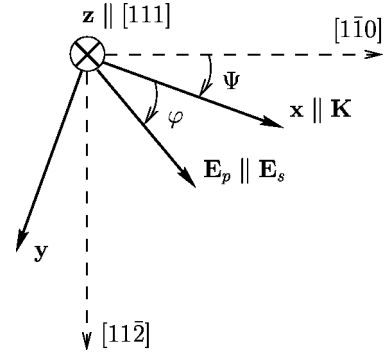
FIG. 3. Geometrical scheme for the optical configuration of (111)-cut crystals.

optimum cut for every crystal thickness. At the same time the corresponding optimum orientations of the grating vector and of the light polarization vector [both of them lie in the (110) plane] depend strongly on the crystal thickness [18,21].

IV. SPECIAL CUT (111)

In the previous section we saw that (110) and (111) are the most interesting crystal cuts. The (110) cut is characterized by the strongest energy exchange while the (111) cut possesses the highest symmetry (for cubic crystals). As we will show, owing to its symmetry properties, the (111) cut allows an easy analytical treatment.

The coupling tensor elements are important factors for wave-mixing. In this section we characterize the coupling tensor for the (111) cut and present it in a convenient form. In Sec. II we have mentioned that there is no restriction on the choice of the x- and y-axis of the laboratory coordinate system. In many cases it is useful to choose the x-axis parallel to the $\mathbf{K}$ vector, so that the light polarization angle is measured from the plane of incidence; this is convenient for experiments. Another possibility, often used for analytical calculations, is to have fixed x- and y-axes. We shall consider a coordinate system which rotates with the grating vector. In such a system the symmetry of the (111) cut is most clearly expressed and a significant simplification of the coupling tensor for BSO and BTO crystals is achieved.

A. Another form of the coupling tensor

Let us choose a laboratory coordinate system with axes $\mathbf{e}_z\|[111]$ and $\mathbf{e}_x$ always parallel to $\mathbf{K}$. The angle Ψ between the $[1\bar{1}0]$ axis and the $\mathbf{K}$ vector (see Fig. 3) indicates the rotation of the grating vector or the coordinate system around the [111] axis.

From Eqs. (4) and (5) we calculate the coupling tensor components, $H_{ij}^{(111)}$, for the (111) cut,

$$H_{ij}^{(111)} = \frac{\sum\limits_k [A_k^{ij}\sin k\Psi + B_k^{ij}\cos k\Psi]}{1 + B_6\cos 6\Psi} + H_{ij}^0. \qquad (9)$$

Here the summation index k takes the values 3 and 9. The coefficients A_k^{ij}, B_k^{ij}, and B_6 depend only on the material constants of the crystals and characterize the elasto-optic ef-

fect. They are given in the Appendix. The parameter H_{ij}^0 in Eq. (9) denotes the components of the coupling tensor without elasto-optic contribution,

$$H_{11}^0 = -H_{22}^0 = \frac{\sqrt{6}}{3}\sin 3\Psi, \quad H_{12}^0 = \frac{\sqrt{6}}{3}\cos 3\Psi. \quad (10)$$

The following symmetry can be checked directly: $H_{ij}^{(111)}(\Psi) = H_{ij}^{(111)}(\Psi \pm 120°) = -H_{ij}^{(111)}(\Psi \pm 180°)$.

B. New form of the coupling tensor for BSO and BTO crystals

The set of Eqs. (9) and (10) is valid for each crystal with cubic symmetry. A useful simplification is possible if we restrict our attention to BSO and BTO. The evaluation of the coefficient B_6 [see Eqs. (A1) in the Appendix] gives $B_6 \simeq -0.04$ for both BSO and BTO. Consequently we can neglect the denominator in the first term of Eq. (9), $1 + B_6 \cos 6\Psi \simeq 1$. Similarly, we obtain for the coefficients A_k^{ij} and B_k^{ij} that $A_3^{11} = 0.35 \gg \{A_9^{11}, B_3^{11}, B_9^{11}\}$, $A_3^{22} = 0.29 \gg \{A_9^{22}, B_3^{22}, B_9^{22}\}$, and $B_3^{12} = 0.11 \gg \{A_3^{12}, A_9^{12}, B_9^{12}\}$ for BSO; $A_3^{22} = 0.24 \gg \{A_9^{22}, B_3^{22}, B_9^{22}\}$ and $1 \gg \{A_k^{11}, B_k^{11}, A_k^{12}, B_k^{12}\}_{k=3,9}$ for BTO. Finally, we rewrite the coupling tensor in the form

$$H_{11}^{(111)} \simeq a_{11}\sin 3\Psi, \quad H_{22}^{(111)} \simeq a_{22}\sin 3\Psi,$$

$$H_{12}^{(111)} \simeq a_{12}\cos 3\Psi, \quad (11)$$

where $a_{11} = \sqrt{6}/3 + A_3^{11}$, $a_{12} = \sqrt{6}/3 + B_3^{12}$, and $a_{22} = -\sqrt{6}/3 + A_3^{22}$ for BSO; $a_{11} = a_{12} = \sqrt{6}/3$ and $a_{22} = -\sqrt{6}/3 + A_3^{22}$ for BTO. The accuracy of this approximation is 2% for BSO and 4% for BTO. The tensor $\mathbf{H}^{(111)}$ in Eq. (11) has the same angular dependence as $\mathbf{H}^0$, except that every element is normalized differently owing to the elasto-optic effect.

A graphical motivation of the above simplification is shown in Fig. 4. We compare the angular dependence of the nonsimplified coupling tensor from Eq. (9) (solid line) with the pure electro-optic tensor $H_{ij}^{(0)}$ (dashed line). As one can see, the role of the elasto-optic effect is different for both crystals. Its contribution to $H_{11}^{(111)}$ and $H_{22}^{(111)}$ for BTO is negligibly small in contrast to BSO where all three coefficients are influenced. However, for both crystals the $H_{ij}^{(111)}$ dependences show practically the same behavior as the H_{ij}^0 dependences but with different amplitudes, which is the base of our approximation. The components of the simplified tensor of Eq. (11) are not plotted in Fig. 4, because they are graphically indistinguishable from the nonsimplified one. Finally, we would like to emphasize that our simplification is valid only in the appropriate coordinate system (Fig. 3).

C. TWM gain in the new representation

The new simplified coupling tensor includes all known effects and can be used with a high degree of accuracy for
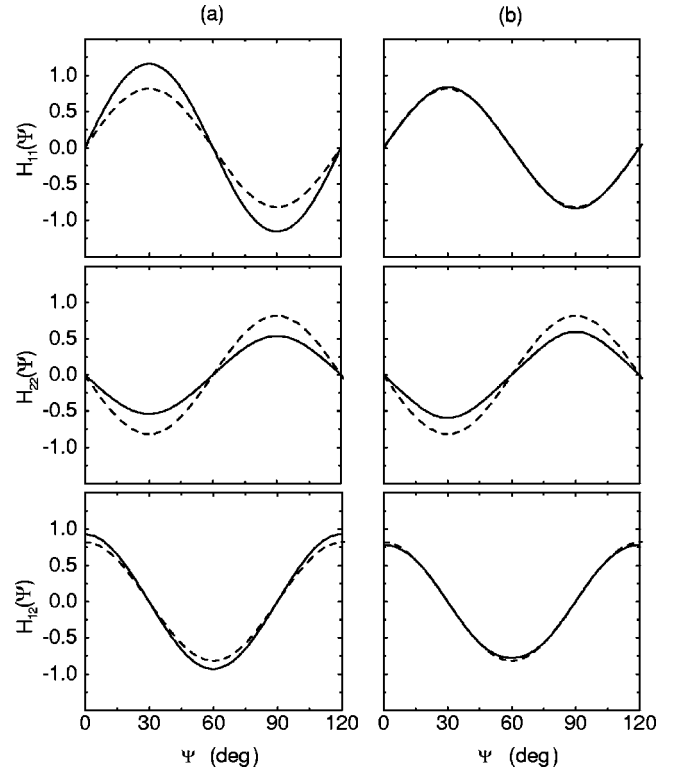
FIG. 4. Dependences of the coupling tensor components $H_{ij}(\Psi)$ for (111)-cut BSO (a), and BTO (b). The dashed lines correspond to the dependences without elasto-optic effect.

the analytical analysis of (111)-cut BSO and BTO crystals. We can, for instance, calculate explicitly the dependence of the gain on the grating vector orientation, Ψ. From Eqs. (8) and (11) we obtain,

$$G = \Gamma d \frac{\beta}{\beta+1}[h_1\sin 3\Psi + h_2\tau\sin 3\Psi\cos(2\varphi - \varrho d)$$

$$+ h_3\tau\cos 3\Psi\sin(2\varphi - \varrho d)], \quad (12)$$

with

$$h_1 = a_{11} + a_{22}, \quad h_2 = a_{11} - a_{22}, \quad h_3 = 2a_{12}.$$

Optimization of Eq. (12) with respect to the polarization angle gives for the maximum gain, $G|_\varphi^{\max}$,

$$G|_\varphi^{\max} = \Gamma d \frac{\beta}{\beta+1}(h_1\sin 3\Psi + |\tau|\sqrt{h_3^2 - (h_3^2 - h_2^2)\sin^2 3\Psi}). \quad (13)$$

The corresponding initial light polarization, φ_{opt}, is

$$\varphi_{opt} - \frac{\varrho d}{2} = \begin{cases} \frac{1}{2}\arctan\left(\frac{h_3}{h_2}\cot 3\Psi\right) + 90° \; \theta(-\sin(\varrho d)\sin(3\Psi)) & \text{for } \tau \neq 0 \\ \text{arbitrary} & \text{for } \tau = 0, \end{cases} \tag{14}$$

where θ is Heaviside's function. It is responsible for the typical 90°-jump of the polarization which characterizes the point where the minimum and the maximum gain are equal [18].

After optimization of Eq. (13) with respect to the angle Ψ we obtain the maximum gain $G_{max}(d)$ and the optimum grating orientation Ψ_{opt} for a given crystal thickness d,

$$G_{max}(d) = \begin{cases} \Gamma d \dfrac{\beta}{\beta+1} \dfrac{h_3(h_1^2 + \tau^2|h_3^2 - h_2^2|)}{\sqrt{\tau^2(h_3^2 - h_2^2)^2 + h_1^2(h_3^2 - h_2^2)}} & \text{for } |\tau| \geqslant \tau_{th} \\[3mm] \Gamma d \dfrac{\beta}{\beta+1}(h_1 + h_2|\tau|) & \text{for } |\tau| < \tau_{th}, \end{cases} \tag{15}$$

$$\Psi_{opt} = \begin{cases} \dfrac{1}{3}\arcsin\dfrac{h_1 h_3}{\sqrt{\tau^2(h_3^2 - h_2^2)^2 + h_1^2(h_3^2 - h_2^2)}} & \text{for } |\tau| \geqslant \tau_{th} \\[3mm] 30° & \text{for } |\tau| < \tau_{th}, \end{cases} \tag{16}$$

where $\tau_{th} = h_1 h_2/|h_3^2 - h_2^2|$. We assumed in the above equations that $\varrho > 0$ and took into account that $h_{1,2,3} > 0$.

In Figs. 5(a) and 5(b) the dependence of Ψ_{opt} and φ_{opt} on the crystal thickness is plotted. For BSO the threshold parameter τ_{th} is greater than one. Since $|\tau| = |\sin(\varrho d)/(\varrho d)|$ is always smaller than one, the optimum grating orientation as well as the initial light polarization for BSO are independent of the crystal thickness. On the other hand, for BTO Ψ_{opt} and φ_{opt} depend on the crystal thickness. Up to $\varrho d \approx 90°$ (e.g., $|\tau| = \tau_{th}$) there are two branches which correspond to the maximum gain. At $|\tau| \leqslant \tau_{th}$ they stick together and the optimum grating orientation and initial light polarization are the same as for BSO, $\Psi_{opt} = 30°$ and $\varphi_{opt} = \varrho d/2$.

Let us now discuss the origin of such behavior. After excluding the elasto-optic contribution in Eqs. (12)–(16) (i.e., putting $h_1 = 0$ and $h_2 = h_3 = 2\sqrt{6}/3$), it can be directly seen that for a given crystal thickness the maximal gain is achieved for arbitrary grating orientation, i.e., $G|_\varphi^{max} = G_{max}(d)$. The presence of the elasto-optic effect gives a preference direction for the energy exchange. Since there is also optical activity, the optimal grating orientation depends in principle on the crystal thickness. The form of this dependence is determined from the ratio between the strengths of the elasto-optic effect and the optical activity.

It is worth mentioning that in some papers [4], the electro-optic and the elasto-optic coefficients for BSO are negative. In this case the energy flow will be in the opposite direction. Consequently, the optimum grating orientation will be rotated by 180° from our result.

Lastly, we will compare our analysis with the already published experimental results from Ref. [22], where TWM measurements are performed in a 2.1-mm-thick (111)-cut BSO crystal with a He-Ne laser (the rotatory power is $\rho = 21.4°$/mm at $\lambda = 633$ nm). The maximum TWM gain is measured when the grating vector is parallel to the $[\bar{1}\bar{1}2]$-axis (with periodicity 120°) and the light polarization

is inclined at 23° to the plane of incidence. In our notation these conditions correspond to $\Psi_{opt} = 30$ and $\varphi_{opt} = 23°$. The theoretical prediction from Eqs. (14) and (16) (see also Fig. 5) gives $\Psi_{opt} = 30$ and $\varphi_{opt} = 22.5°$. This result is in very good agreement with the experiment.

V. CONCLUSIONS

We investigated TWM in cubic crystals. In this study all known effects were taken into account: optical activity,
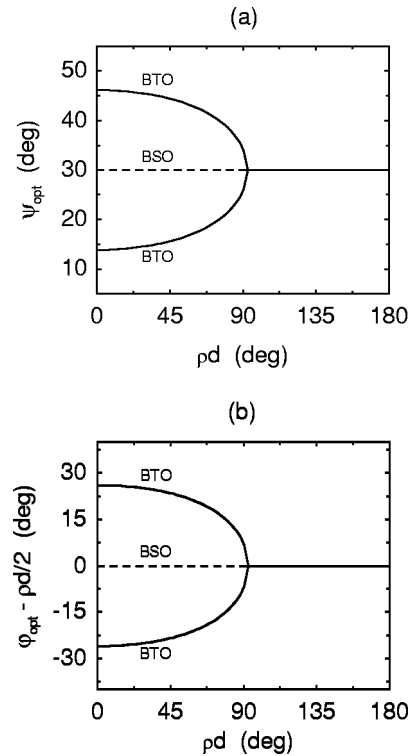
FIG. 5. Dependences $\Psi_{opt}(\rho d)$ (a) and $\varphi_{opt}(\rho d)$ (b) for BSO (dashed line) and BTO (solid line).

electro-optic effect, and elasto-optic effect. We showed that the (110) cut corresponds to the largest possible TWM gain even if optical activity and the elasto-optic effect are taken into account. We derived a simple analytical expression for the components of the coupling tensor of (111)-cut BTO and BSO crystals which allowed us to optimize the TWM gain analytically with respect to the grating orientation and the initial light polarization.

APPENDIX

For (111)-cut cubic crystals the coupling tensor H_{ij} in the coordinate system shown in Fig. 3 is given by Eq. (9). The corresponding coefficients are

$$A_3^{11} = \frac{\sqrt{6}}{648} \frac{e_{41}}{r_{41}} \left[p_1 a_1 + \left(\frac{p_2 + p_3}{2} + 2p_4 \right) a_2 \right], \quad \text{(A1)}$$

$$A_3^{22} = \frac{\sqrt{6}}{648} \frac{e_{41}}{r_{41}} \left[(p_1 - 2p_4) a_4 + \frac{p_2 + p_3}{2} a_5 \right],$$

$$A_9^{11} = -A_9^{22} = B_9^{12} = \frac{\sqrt{6}}{648} \frac{e_{41}}{r_{41}} \left(p_1 - \frac{p_2 + p_3}{2} - 2p_4 \right) a_3,$$

$$A_3^{12} = \frac{\sqrt{2}}{432} \frac{e_{41}}{r_{41}} (p_2 - p_3) a_6,$$

$$B_3^{11} = -B_9^{11} = -B_3^{22} = B_9^{22} = A_9^{12} = \frac{\sqrt{2}}{432} \frac{e_{41}}{r_{41}} (p_2 - p_3) a_3,$$

$$B_3^{12} = \frac{\sqrt{6}}{648} \frac{e_{41}}{r_{41}} \left[-\left(p_1 - \frac{p_2 + p_3}{2} \right) a_3 + 2p_4 a_7 \right],$$

$$B_6 = -\frac{1}{108b} (c_1 + 2c_2 + c_4)(c_1 - c_2 - 2c_4)^2,$$

where a_i and b are combinations of the elasticity moduli c_i,

$$a_1 = 3(c_1^2 + 4c_2^2 - 2c_4^2 - 5c_1c_2 + 5c_1c_4 - 11c_2c_4)/b,$$

$$a_2 = 3(5c_1^2 + 2c_2^2 + 2c_4^2 - 7c_1c_2 + 19c_1c_4 - 13c_2c_4)/b,$$

$$a_3 = -(c_1 + 2c_2 + c_4)(c_1 - c_2 - 2c_4)/b,$$

$$a_4 = 3(3c_1^2 + 2c_4^2 - 3c_1c_2 + 11c_1c_4 - 5c_2c_4)/b,$$

$$a_5 = 3(3c_1^2 + 6c_2^2 - 2c_4^2 - 9c_1c_2 + 13c_1c_4 - 19c_2c_4)/b,$$

$$a_6 = -3(c_1 + 2c_2 + c_4)(c_1 - c_2 + 2c_4)/b,$$

$$a_7 = (26c_1^2 - 25c_2^2 + 2c_4^2 - c_1c_2 + 55c_1c_4 - 49c_2c_4)/b,$$

$$b = c_1c_4^2 + \frac{1}{108}(c_1 - c_2 - 2c_4)[27c_4(c_1 + c_2)$$

$$+ (c_1 + 2c_2 + c_4)(c_1 - c_2 - 2c_4)].$$

[1] L. Solymar, D.J. Webb, and A. Grunnet-Jepsen, *The Physics and Applications of Photorefractive Materials* (Clarendon, Oxford, 1996).

[2] M.P. Petrov, S.I. Stepanov, and A.V. Khomenko, *Photorefractive Crystals in Coherent Optical Systems*, Springer Series in Optical Sciences, Vol. 59 (Springer-Verlag, Heidelberg, Germany, 1991).

[3] A.A. Izvanov, A.E. Mandel, N.D. Khatkov, and S.M. Shandarov, Avtometriya No. 2, 79 (1986) [Optoelectron. Data Process. Instrum. No. 2, 80 (1986)].

[4] S. Stepanov, S.M. Shandarov, and N.D. Khat'kov, Sov. Phys. Solid State **29**, 1754 (1987).

[5] A.E. Mandel, S.M. Shandarov, and V.V. Shepelevich, Opt. Spectrosc. **67**, 481 (1989).

[6] V.V. Shepelevich, S.M. Shandarov, and A.E. Mandel, Ferroelectrics **110**, 235 (1990).

[7] S.M. Shandarov, V.V. Shepelevich, and N.D. Khatkov, Opt. Spectrosc. **70**, 627 (1991).

[8] V.V. Shepelevich, and N.N. Egorov, Opt. Spectrosc. **71**, 600 (1991).

[9] N.V. Kukhtarev, T.I. Semenec, and P. Hribek, Ferroelectr. Lett. Sect. **13**, 29 (1991).

[10] G. Pauliat, P. Mathey, and G. Roosen, J. Opt. Soc. Am. B **8**, 1942 (1991).

[11] S.M. Shandarov, Appl. Phys. A: Solids Surf. **55**, 91 (1992).

[12] E. Anastassakis, IEEE J. Quantum Electron. **29**, 2239 (1993).

[13] V.V. Shepelevich, N.N. Egorov, and V. Shepelevich, J. Opt. Soc. Am. B **11**, 1394 (1994).

[14] R. Litvinov, and S. Shandarov, J. Opt. Soc. Am. B **11**, 1204 (1994).

[15] H.C. Ellin and L. Solymar, Opt. Commun. **130**, 85 (1996).

[16] S.M. Shandarov, A. Emelyanov, O. Kobozev, A. Reshet'ko, V.V. Volkov, and Y.F. Kargin, Proc. SPIE **2801**, 221 (1996).

[17] V.V. Shepelevich, Opt. Spectrosc. **83**, 161 (1997).

[18] E. Shamonina, V.P. Kamenov, K.H. Ringhofer, G. Cedilnik, A. Kiessling, and R. Kowarschik, J. Opt. Soc. Am. B **15**, 2552 (1998).

[19] S. Stepanov, N. Korneev, A. Gerwens, and K. Buse, Appl. Phys. Lett. **72**, 879 (1998).

[20] M.P. Petrov, A.P. Paugurt, V.V. Bryksin, and V.M. Petrov, Tech. Phys. Lett. **24**, 873 (1998).

[21] V.V. Shepelevich, Y. Hu, A. Firsov, E. Shamonina, and K.H. Ringhofer, Appl. Phys. B: Lasers Opt. **68**, 923 (1999).

[22] V.V. Shepelevich, S.F. Nichiporko, A.E. Zagorskiy, N.N. Egorov, Y. Hu, K.H. Ringhofer, and E. Shamonina, in *Advances in Photorefractive Materials, Effects, and Devices*, edited by Andersen, Johansen, Pedersen, Petersen, and Saffman, OSA TOPS **27**, 353 (1999).

[23] M.P. Georges and P.C. Lemaire, in *Proceedings of the Topical Meeting in Photorefractive Materials, Effects, and Devices* (Optical Society of Japan, Tokyo, Japan, 1997), pp. 495–498 and 637–640.

[24] B. Sugg, F. Kahmann, R.A. Rupp, P. Delaye, and G. Roosen, Opt. Commun. **102**, 6 (1993).

[25] N. Kukhtarev, B.S. Chen, P. Venkateswarlu, G. Salamo, and M. Klein, Opt. Commun. **104**, 23 (1993).

[26] Y. Ding and H.J. Eichler, Opt. Commun. **110**, 456 (1994).

[27] H.J. Eichler, Y. Ding, and B. Smandek, Phys. Rev. A **52**, 2411 (1995).